Journal of Analysis and Testing (2019) 3:228–237
https://doi.org/10.1007/s41664-019-00100-4

ORIGINAL PAPER

Pyrophosphate-Mediated On–Off–On Oxidase-Like Activity Switching of Nanosized $MnFe_2O_4$ for Alkaline Phosphatase Sensing

Xiangheng Niu[1] · Kun Ye[1] · Zhibo Li[1] · Hongli Zhao[2] · Linjie Wang[1] · Jianming Pan[1] · Hongwei Song[3] · Minbo Lan[2]

Received: 1 March 2019 / Accepted: 8 April 2019 / Published online: 22 April 2019

Abstract

Developing reliable and facile approaches for alkaline phosphatase (ALP) sensing is important due to its role as a clinical biomarker for many diseases. In this study, we proposed a new and convenient colorimetric assay based on the pyrophosphate (PPi)-mediated oxidase-mimicking activity switching of nanosized $MnFe_2O_4$ for the detection of ALP. The synthesized $MnFe_2O_4$ exhibited high oxidase-like activity to catalyze the oxidation of colorless 3,3′,5,5′-tetramethylbenzidine (TMB) to its blue product TMBox in the presence of dissolved O_2, leading to a color reaction rapidly and remarkably; PPi could significantly inhibit the activity of the $MnFe_2O_4$ nanozyme via the strong interaction between PPi and the Fe(III) species in $MnFe_2O_4$, resulting in the suppression of the TMB color reaction; when ALP was added, it hydrolyzed the PPi substrate to phosphate (Pi) that had no obvious effect on the $MnFe_2O_4$ activity, and such that the TMB color reaction catalyzed by the nanozyme could be observed again. With the above principle, linear colorimetric determination of ALP in the scope of 0.6–55 U L^{-1} was achieved, giving the limit of detection down to 0.27 U L^{-1}. Besides, the developed assay could provide selective response toward ALP against other co-existing biological species. Furthermore, reliable detection of ALP in human serum samples was verified by our assay, revealing its great promise as an effective and facile tool for ALP monitoring in clinical practice.

Keywords Oxidase-like nanozyme · Activity switching · PPi · ALP · Colorimetric analysis

1 Introduction

Alkaline phosphatase (ALP) is a glucoproteinase that has the specific catalysis for the dephosphorylation process of lots of biological substances, including small molecules, nucleic acids, and proteins. Previous researches have confirmed that the abnormality of ALP activity or concentration can lead to a great variety of diseases, such as liver dysfunction [1], bone injury [2], and prostate cancer [3]. In clinical practice, it has become an important biomarker for the diagnosis of these diseases. Thus, it is of great significance to develop effective and simple methods for ALP monitoring [4–8].

Up to now, several approaches, including colorimetric [8–17], fluorometric [6, 7, 18–20], electrochemical [21, 22], and Raman [23, 24] means, have been exploited for the analysis of ALP based on its ability of removing the phosphate group from substrates to gain signal readouts via various principles. Among these approaches, colorimetric assays have drawn considerable interest because of their merits of simplicity, easy readout, and low cost [8, 25]. At present, the hydrolysis of colorless *p*-nitrophenyl

Electronic supplementary material The online version of this article (https://doi.org/10.1007/s41664-019-00100-4) contains supplementary material, which is available to authorized users.

✉ Xiangheng Niu
niuxiangheng@126.com

✉ Jianming Pan
pjm@ujs.edu.cn

✉ Minbo Lan
minbolan@ecust.edu.cn

[1] Institute of Green Chemistry and Chemical Technology, School of Chemistry and Chemical Engineering, Jiangsu University, Zhenjiang 212013, China

[2] Shanghai Key Laboratory of Functional Materials Chemistry, School of Chemistry and Molecular Engineering, East China University of Science and Technology, Shanghai 200237, China

[3] School of Environmental and Chemical Engineering, Jiangsu University of Science and Technology, Zhenjiang 212003, China

phosphate (*p*-NPP) to yellow *p*-nitrophenolate (*p*-NP) is universally used to monitor ALP in clinical practice [26]. Although this type of assay is simple, the poor selectivity significantly limits its practicality. More seriously, the *p*-NPP substrate is so sensitive to light and heat that it can be hydrolyzed without the participation of ALP, which will produce false-positive results [27]. Therefore, it still needs further effort to explore novel mechanisms and approaches with good practicability and reliability for the determination of ALP.

Since Yan's group found that magnetic Fe_3O_4 particles exhibited intrinsic peroxidase-like activity in 2007 [28], nanozymes, defined as nanoscale materials with enzyme-mimicking properties, have attracted increasing attention in the academic community [29–34]. With the superiorities of large-scale production, low cost, good robustness, and easy-to-adjust performance compared with natural enzymes, they have been developed for use in catalysis [35, 36], biomedicine [37–39], and sensing [40–49]. For the detection of ALP, several nanozymes or enzyme mimics have found promising applications on the basis of various principles [4, 8, 12, 17, 50–52]. For example, Wang's group used ALP to hydrolyze the *o*-phosphonoxyphenol substrate to catechol that could stimulate the inert TiO_2 nanoparticles to a photoresponsive nanozyme, and with this strategy ultrasensitive monitoring of ALP was gained [12]. Liu et al. developed a fluorescent and colorimetric dual-mode ALP assay based on the destruction of oxidase-like CoOOH nanoflakes by ascorbic acid generated from an ALP-catalyzed dephosphorylation process [50]. Very recently, we reported a sensitive and selective strategy based on the phosphate-quenched oxidase-mimicking activity of Ce(IV) ions for the colorimetric detection of ALP [8]. These successful cases suggest that nanozymes with adjustable activities have great potential in the ALP monitoring application.

Herein, we propose a new colorimetric assay based on the pyrophosphate (PPi)-mediated oxidase-mimicking activity switching of nanosized $MnFe_2O_4$ for ALP analysis. As illustrated in Scheme 1, nanosized $MnFe_2O_4$ was synthesized and used as an oxidase-like nanozyme with high activity to catalyze the oxidation of colorless 3,3′,5,5′-tetramethylbenzidine (TMB) to blue TMBox, providing a remarkable color reaction rapidly; PPi was found to inhibit the nanozyme activity through the strong interaction of PPi and the Fe(III) species in $MnFe_2O_4$, and such that the TMB color reaction was suppressed seriously; when ALP existed, it hydrolyzed the PPi substrate to phosphate (Pi) that showed no notable influence on the $MnFe_2O_4$ activity, and as a result the nanozyme-catalyzed TMB color reaction could be observed again. With this principle, sensitive and selective analysis of ALP was obtained. Reliable monitoring of the target in clinical samples was also verified by our developed assay.

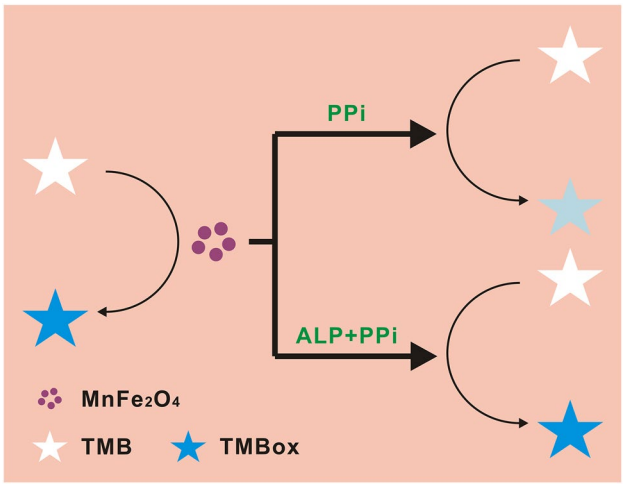

Scheme 1 Illustration of the colorimetric detection of ALP based on the PPi-mediated oxidase-like activity switching of nanosized $MnFe_2O_4$

2 Experimental Section

2.1 Chemicals and Reagents

$FeCl_3{\cdot}6H_2O$, $MnSO_4{\cdot}H_2O$, $NH_3{\cdot}H_2O$, $Na_4P_2O_7{\cdot}10H_2O$, and Na_3PO_4 were obtained from Sinopharm Chemical Regent Co., Ltd. TMB was provided by Shanghai Macklin Biochemical Co., Ltd. ALP (30 U mg^{-1}, from *Escherichia coli*), cysteine, glycine, alanine, glutathione, bovine serum albumin, glucose, dopamine, cholesterol, and cholesterol oxidase (ChOx, 10 U mg^{-1}) were purchased from Shanghai Aladdin Reagent Co., Ltd. Glucose oxidase (GOx, 100 U mg^{-1}, from *Aspergillus niger*) was obtained from Sigma-Aldrich. Urate oxidase (UOx, 10 U mg^{-1}, from *Arthrobacter protophormiae*) was provided by Beijing Bailingwei Technology Co., Ltd. All the other chemicals and reagents were of analytical grade and used directly. Deionized water was employed during the whole study.

2.2 Synthesis and Characterization of $MnFe_2O_4$

The $MnFe_2O_4$ nanozyme was prepared via a simple co-precipitation method similar to our previous report [53]. In detail, 1 mM $FeCl_3$ and 0.5 mM $MnSO_4$ were first dissolved in 30 mL deionized water; then the mixture was bubbled with pure N_2 for 30 min to expel the dissolved O_2; afterwards, 20 mL $NH_3{\cdot}H_2O$ was rapidly added to the mixture with a continuously vigorous stir; after reaction for 2 h, the formed solids were rinsed with adequate deionized water until the leachate pH is nearly neutral, and the products were collected via centrifugation and dried for use.

The synthesized $MnFe_2O_4$ was characterized by X-ray diffraction (XRD) measurements on a 6100 diffractometer (Shimadzu). High-resolution transmission electron microscopy (HRTEM) images were obtained using a JEM-2100 microscope (JEOL). X-ray photoelectron spectroscopy (XPS) measurements were done with an ESCALAB-MKII spectrometer (Thermo-Fisher Scientific Co., Ltd.).

2.3 Evaluation of the Oxidase-Like Activity of Nanosized $MnFe_2O_4$

To evaluate the oxidase-like activity of the synthesized $MnFe_2O_4$, TMB was employed as a chromogenic substrate. 1 mg mL^{-1} $MnFe_2O_4$ stock solution was prepared with deionized water, and 5 mM TMB stock solution was prepared with ethanol. In detail, 50 µL $MnFe_2O_4$ solution was first added to 1.85 mL NaAc-HAc buffer (0.2 M, pH 4.0), and 100 µL TMB solution was further added to the above solution and mixed uniformly for reaction. The UV–Vis spectra of the mixture were monitored by a Cary 8454 spectrometer (Agilent Technologies Co., Ltd.). Steady-state kinetic measurements were carried out by recording the absorbance at 652 nm within 1 min at a 5 s interval. The apparent kinetic parameters were determined according to the Michaelis–Menten equation $\upsilon = V_{max}[S]/(K_m + [S])$, where υ represents the reaction velocity, V_{max} is the maximum velocity, [*S*] represents the concentration of TMB, and K_m is the Michaelis–Menten constant.

2.4 Detection of ALP Based on the PPi-Mediated Oxidase-Like Activity Switching of Nanosized $MnFe_2O_4$

To investigate the influences of PPi and Pi on the oxidase-mimicking activity of the synthesized $MnFe_2O_4$, 50 µL $MnFe_2O_4$ solution and 50 µL PPi or Pi solutions (10 mM) were first added to 1.8 mL NaAc-HAc buffer (0.2 M, pH 4.0) and mixed uniformly, and then 100 µL TMB solution was added to the above solution for reaction. The mixture was monitored by the UV–Vis spectrometer.

For the colorimetric detection of ALP on the basis of the PPi-mediated oxidase-like activity switching of nanosized $MnFe_2O_4$, 50 µL ALP solution (Tris–HCl buffer, 0.1 M, pH 8.5) with a certain activity and 50 µL PPi solution (10 mM) were first incubated at 37 °C for 40 min, and then 1.8 mL NaAc-HAc buffer (0.2 M, pH 4.0) was added to the mixture. After that, 100 µL TMB solution was added to the above solution for further reaction for 10 min. The mixture was also monitored by the UV–Vis spectrometer.

For the detection of ALP in real samples, human serum samples obtained from the Affiliated Hospital of Jiangsu University were measured using our assay. In detail, 50 µL PPi solution (10 mM) and 50 µL serum sample were first incubated in a tube at 37 °C for 40 min, and then 1.8 mL NaAc-HAc buffer (0.2 M, pH 4.0) was added to the tube. After that, 100 µL TMB solution was added to the above tube. After reaction for 10 min, the mixture was detected by UV–Vis.

3 Results and Discussion

3.1 Characterization of the Synthesized $MnFe_2O_4$

The synthesized material was characterized by several means. Figure 1a presents the XRD pattern of the collected products. Three ambiguous peaks attributed to the (311), (400), and (440) planes of spinel $MnFe_2O_4$ (JCPDS No. 10-0319) are observed. These indefinable diffraction signals reveal that the $MnFe_2O_4$ material prepared by the co-precipitation method has a poor crystallinity, which is in accordance with the previous study [53]. The HRTEM image (Fig. 1b) does not provide long-range ordered crystal structures. Instead, only some short-range lattice fringes are observed in the HRTEM image. This result also supports the poor crystallinity of the synthesized $MnFe_2O_4$. As demonstrated by the full XPS (Fig. 1c), both Fe and Mn are present in the obtained material. In the Mn 2p XPS (Fig. 1d), the four fitting peaks centered at 654.7, 653.5, 643.8, and 642.3 eV are ascribed to Mn^{4+} $2p_{1/2}$, Mn^{2+} $2p_{1/2}$, Mn^{4+} $2p_{3/2}$, and Mn^{2+} $2p_{3/2}$, respectively. This result suggests the coexistence of Mn^{2+} and Mn^{4+} in the synthesized $MnFe_2O_4$. The Mn^{4+} species is supposed to originate from the redox reaction between the Mn^{2+} and Fe^{3+} precursors during synthesis [54].

3.2 Oxidase-Like Activity of the Synthesized $MnFe_2O_4$

Previous studies have revealed that Mn-based materials exhibits oxidase-mimicking activity to trigger some chromogenic reactions [55, 56]. Since our synthesized $MnFe_2O_4$ has the Mn^{4+} and Mn^{2+} species, as demonstrated by Fig. 1d, it is also expected to provide oxidase-like catalytic activity. To check the guess, we used the synthesized $MnFe_2O_4$ to catalyze the oxidation of TMB, a chromogenic substrate that is commonly used to evaluate the enzyme-like characteristics of nanozymes. As compared in Fig. 2a, the $MnFe_2O_4$ solution with a concentration of 0.025 mg mL^{-1} has no obvious color background, and the TMB substrate also exhibits no UV–Vis signal. When the synthesized $MnFe_2O_4$ and TMB are incubated together, a color reaction occurs fast, providing a remarkable absorption peak at around 652 nm. The reaction should be attributed to the oxidation of colorless TMB to its blue product TMBox. This result verifies that the synthesized $MnFe_2O_4$ has oxidase-mimicking activity.

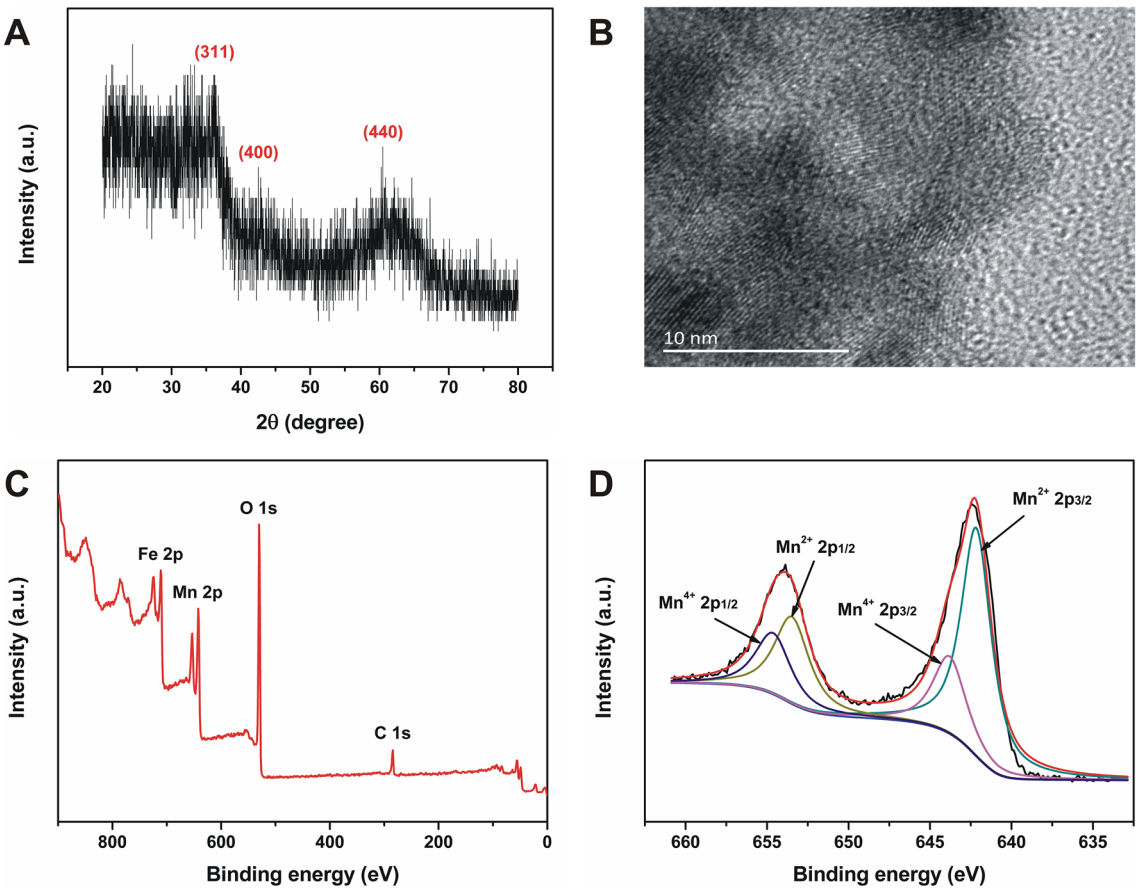

Fig. 1 **a** Shows the XRD pattern of the synthesized $MnFe_2O_4$. **b** Displays the HRTEM image of nanosized $MnFe_2O_4$. **c** Shows the full XPS of the synthesized material. **d** Exhibits the Mn 2p XPS of $MnFe_2O_4$

To confirm that the synthesized $MnFe_2O_4$ indeed plays an oxidase-mimicking role to trigger the TMB color reaction but not acts as an oxidant, the $MnFe_2O_4$ + TMB system occurring in air- or N_2-saturated solutions was compared [57]. As depicted in Fig. 2b, the colorless TMB substrate can be catalytically oxidized to blue TMBox fast in the air-saturated buffer, while in the N_2-saturated buffer the TMB color reaction is seriously inhibited. This contrast verifies that the obtained $MnFe_2O_4$ indeed plays an oxidase-like nanozyme role rather than simply an oxidant [57]. The oxidase-mimicking activity of $MnFe_2O_4$ is supposed to originate from the Mn species, because it has been reported to have oxidase-like activity [55, 56] but not the Fe species. To verify this conclusion, we synthesized Fe_3O_4 nanoparticles using a similar method and tested their enzyme-like characteristics. As demonstrated in Figure S1 (Supplementary Information), Fe_3O_4 nanoparticles exhibit no ability to trigger the TMB color reaction with the absence of H_2O_2. The result clarifies that the oxidase-mimicking activity of $MnFe_2O_4$ is indeed attributed to the Mn species. In detail, the Mn species exhibits both the Mn^{4+} and Mn^{2+} oxidation states (Fig. 1d). It is supposed that an initial oxidation of Mn^{2+} to Mn^{4+} first occurs with the reduction of O_2 to H_2O, and then the oxidation of TMB by Mn^{4+} leads to the regeneration of Mn^{2+} [54], thus giving the oxidase-like ability of the $MnFe_2O_4$ nanomaterial.

Similar to other nanozymes, the oxidase-mimicking activity of the proposed $MnFe_2O_4$ highly depends on the pH value of the buffer used. As presented in Figure S2 (Supplementary Information), with the increasing pH of the buffer in the range of 3–9, the absorbance of the $MnFe_2O_4$ + TMB system first increases and then decreases, providing the maximal absorbance at pH 4. The TMB color reaction catalyzed by the $MnFe_2O_4$ nanozyme also changes along with the reaction temperature. A volcano-type trend between the oxidase-like activity and the reaction temperature is observed in Figure S3 (Supplementary Information). For the convenience of measurements, the following experiments were carried out at room temperature.

To better assess the oxidase-mimicking activity of the proposed $MnFe_2O_4$, steady-state kinetic measurements were carried out under optimized conditions. As presented in Fig. 2c, typical Michaelis–Menten plots are found for the TMB substrate, providing a K_m value of 0.23 mM and

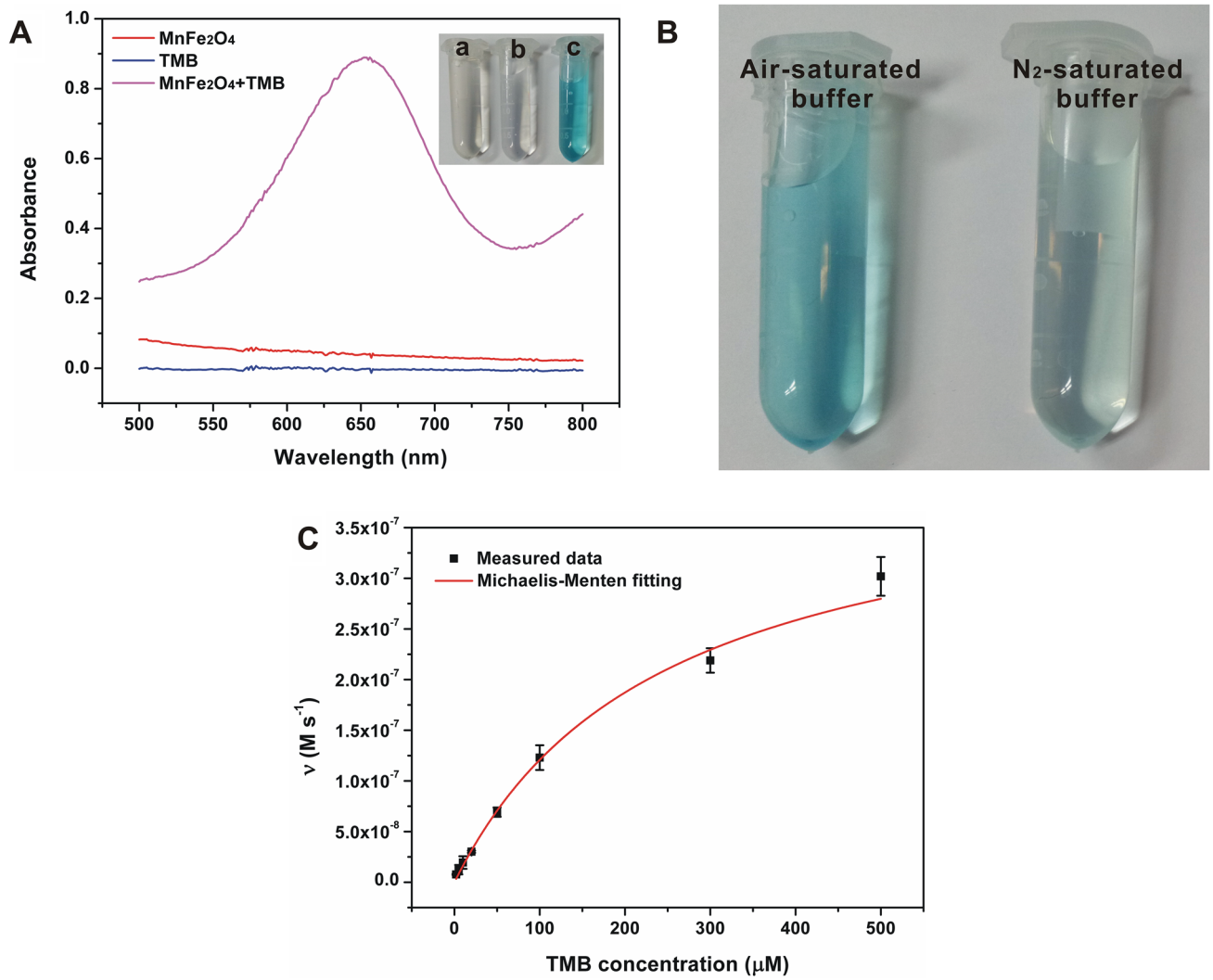

Fig. 2 **a** Compares the UV–Vis spectra of different systems, and the inset shows the corresponding photograph (a—$MnFe_2O_4$, b—TMB, c—$MnFe_2O_4$ + TMB). **b** Presents the photograph of the $MnFe_2O_4$ + TMB system occurring in air- or N_2-saturated solutions. **c** Shows the steady-state kinetic plots of the $MnFe_2O_4$ nanozyme toward TMB

a V_{max} value of 4.17×10^{-7} M s^{-1} when the concentration of $MnFe_2O_4$ utilized is 0.025 mg mL^{-1}. According to the literature [58], the catalytic constant k_{cat} and efficiency k_{cat}/K_m are further determined to be 3.86×10^{-3} s^{-1} and 16.78 M^{-1} s^{-1}, respectively. Although the catalytic efficiency of the $MnFe_2O_4$ nanozyme is still inferior in comparison with natural oxidase, it shows advantages of large-scale preparation, low cost, and good robustness. In addition, the $MnFe_2O_4$ nanozyme, similar to other nanozymes, shows excellent stability against harsh conditions. When it is first incubated at different temperatures (Figure S4, Supporting Information) or in buffers with various pH values (Figure S5, Supporting Information) for a certain time and then tested, its enzymatic activity has no remarkable changes, revealing the favorable robustness of the $MnFe_2O_4$ nanozyme.

3.3 The Oxidase-Like Activity of $MnFe_2O_4$ can be Inhibited by PPi but not Pi

It is interestingly found that the oxidase-like activity of the synthesized $MnFe_2O_4$ nanozyme can be inhibited by PPi. As depicted in Fig. 3a, the $MnFe_2O_4$ + TMB system triggers a remarkable color reaction fast. When 0.25 mM PPi is added, the color reaction is seriously restrained. Given that the PPi species cannot directly affect the TMB and TMBox substances, the suppression should only be ascribed to the inhibition of the $MnFe_2O_4$ nanozyme activity. Previous studies have confirmed that PPi is able to chelate certain metal ions including Fe^{3+} and Cu^{2+} [36, 59]. Therefore, it is supposed that the activity inhibition of the $MnFe_2O_4$ nanozyme originates from the strong coordination interaction between PPi and the Fe(III) species in

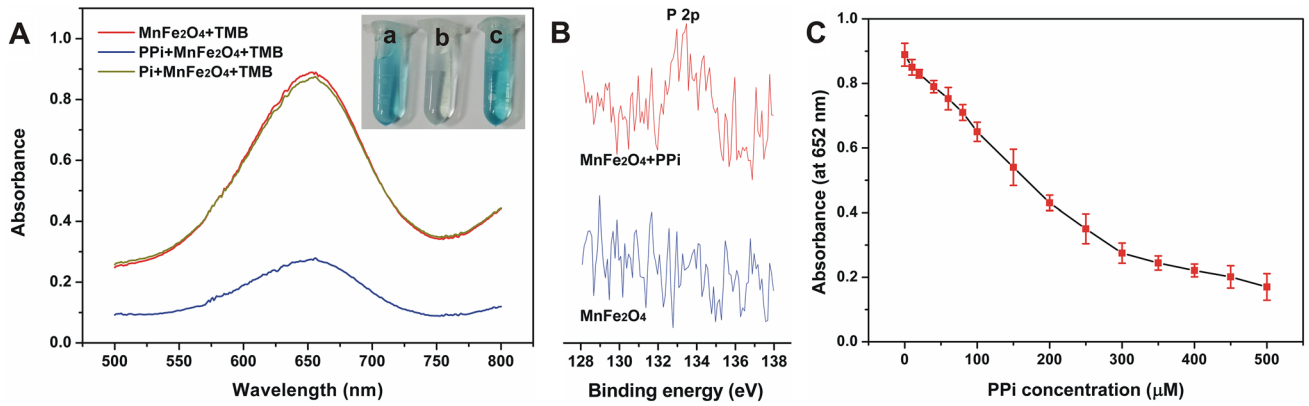

Fig. 3 **a** Compares the UV–Vis spectra of the $MnFe_2O_4$ + TMB system with/without the addition of PPi or Pi (TMB: 0.25 mM; $MnFe_2O_4$: 25 μg mL^{-1}), and the inset shows the corresponding photograph (a—$MnFe_2O_4$ + TMB, b—$MnFe_2O_4$ + PPi + TMB, c—$MnFe_2O_4$ + Pi + TMB). **b** Compares the P 2p XPS of the synthesized $MnFe_2O_4$ before and after interacting with PPi. **c** Indicates that the suppression degree of the $MnFe_2O_4$ + TMB system by PPi highly depends on the concentration of PPi added

$MnFe_2O_4$. To back the hypothesis, the $MnFe_2O_4$ nanozyme before and after interacting with PPi was characterized by XPS. As shown in Fig. 3b, in the as-synthesized $MnFe_2O_4$ no P 2p signal is detected. After incubating with PPi, the collected material offers a weak but recognizable P 2p signal. This result demonstrates that the PPi species indeed combines with the $MnFe_2O_4$ nanozyme.

However, when Pi, instead of PPi, is added, the TMB color reaction can be observed as that with no addition of Pi (Fig. 3a). The result reveals that the Pi species barely affects the nanozyme activity, different from the previous study reporting that Pi could suppress the peroxidase-like activity of magnetite nanoparticles (MNPs) [60]. The difference may be related to the two nanozymes used. In the previous study [60], Pi could weakly coordinate with Fe^{3+} on the surface of MNPs, and the Fe^{3+} species played the main peroxidase-mimicking role. Therefore, Pi with a high concentration might be able to inhibit the catalytic activity of MNPs. In our work, Pi may also weakly coordinate with Fe^{3+} in $MnFe_2O_4$, but the species with a smaller molecular structure compared with PPi cannot affect the nearby Mn^{2+}/Mn^{4+} species (which play the main oxidase-mimicking role) as PPi does. Besides, in comparison with the coordination of Fe^{3+} and PPi, the interaction between Pi and Fe^{3+} is much weaker. Therefore, no obvious influence of Pi (with a concentration of 0.25 mM) on the catalytic activity of the $MnFe_2O_4$ nanozyme is found, while PPi with the same concentration can significantly inhibit the nanozyme-catalyzed TMB color reaction. It is further found that the suppression degree of the $MnFe_2O_4$ + TMB system by PPi highly depends on the concentration of the latter. With the increase of the PPi concentration, the $MnFe_2O_4$ + TMB system is inhibited more significantly, resulting in the decreasing absorbance at 652 nm, as observed in Fig. 3c.

3.4 Colorimetric Detection of ALP Based on the PPi-Mediated Oxidase-Like Activity Switching of $MnFe_2O_4$

With the above finding, a colorimetric assay based on the PPi-mediated oxidase-like activity switching of $MnFe_2O_4$ was explored for the monitoring of ALP. As illustrated in Scheme 1, PPi can inhibit the TMB color reaction catalyzed by the $MnFe_2O_4$ nanozyme; it is expected that ALP will hydrolyze the PPi substrate to Pi that cannot affect the nanozyme, and such that the TMB color reaction can be observed again. To verify the assay, the UV–Vis spectra of the PPi + $MnFe_2O_4$ + TMB and ALP + PPi + $MnFe_2O_4$ + TMB systems were compared. As

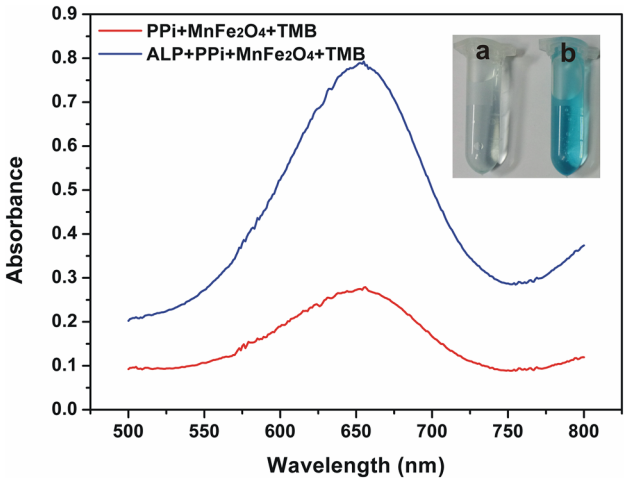

Fig. 4 UV–Vis spectra of the PPi + $MnFe_2O_4$ + TMB system with the presence of ALP or not (PPi: 5 mM; TMB: 0.25 mM; $MnFe_2O_4$: 25 μg mL^{-1}). The inset shows the corresponding photograph (a—PPi + $MnFe_2O_4$ + TMB, b—ALP + PPi + $MnFe_2O_4$ + TMB)

shown in Fig. 4, it is obvious that the presence of ALP can restore the nanozyme-catalyzed TMB color reaction. The phenomenon can be utilized for the colorimetric determination of ALP.

To detect ALP better, the reaction time of ALP and PPi was optimized. Figure S6 (Supplementary Information) depicts the effect of the reaction time between ALP and PPi on the signal readout. When the reaction time extends, the absorbance at 652 nm also increases until a saturation phenomenon appears when the reaction time extends to 40 min. Finally, we selected 40 min as the optimal reaction time of ALP and PPi.

Under optimized conditions, we utilized the developed assay to detect the ALP target with different activities. As expected, the UV–Vis responses of the ALP + PPi + $MnFe_2O_4$ + TMB system increase along with the increasing activities of ALP (Fig. 5a). It is further found that the absorbance at 652 nm is linearly increased with the ALP activity ranging from 0.6 to 55 U L^{-1}. Based on the signal-to-noise of three ($S/N = 3$) rule, the limit of detection (LOD) for ALP determination is determined to be as low as 0.27 U L^{-1}. The detection range and LOD can fully meet the requirements for ALP monitoring in clinical practice. In comparison with previously reported assays for ALP sensing (Table S1, Supplementary Information), our assay is also comparable or even better in terms of linear range and LOD. More importantly, our assay exhibits the following merits over other methods: (1) compared with fluorescence measurements that usually need some labels [5, 18, 61], our colorimetric assay can offer comparable analytical performance with simpler sensing elements, and smartphone or even naked eyes can

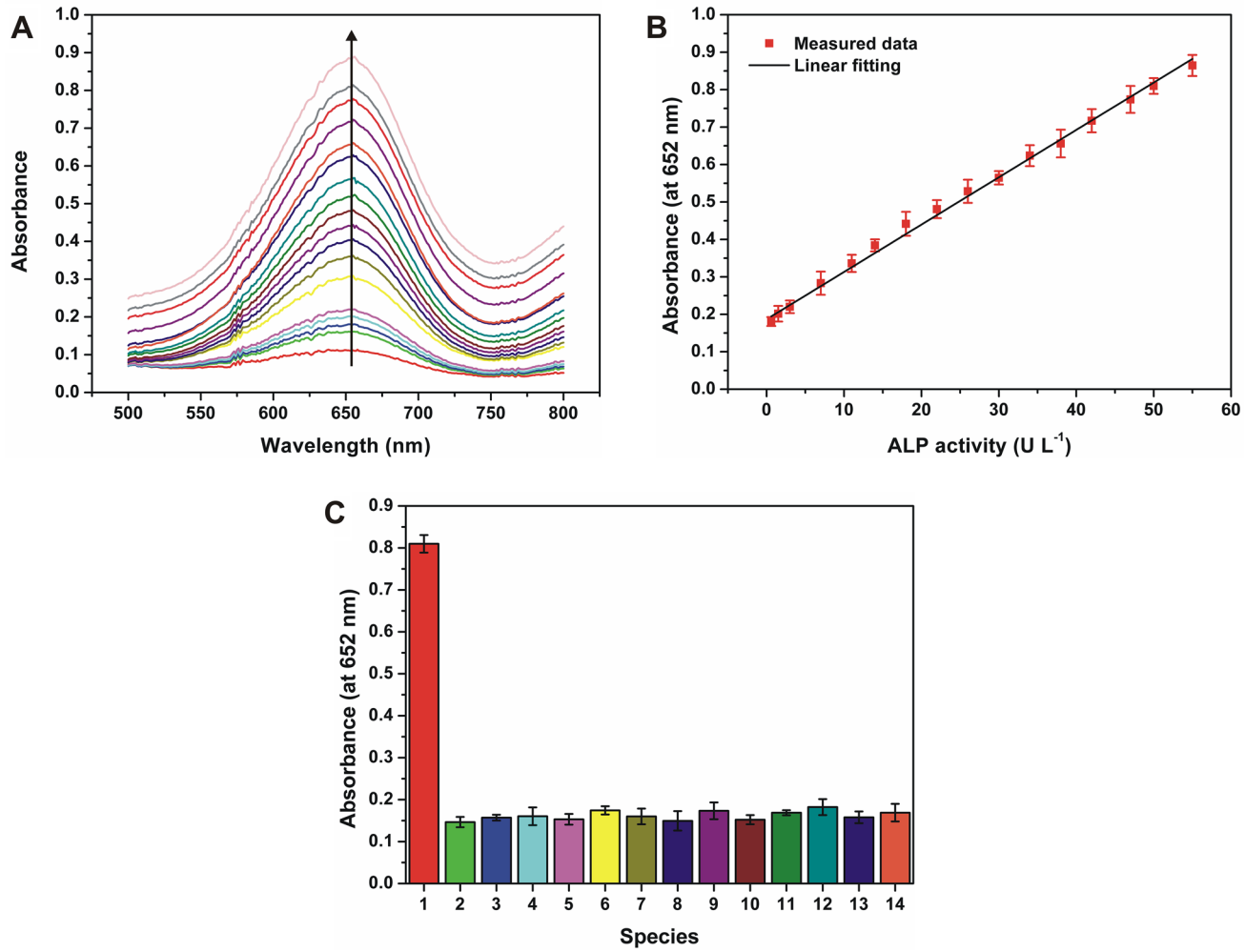

Fig. 5 **a** Shows the UV–Vis spectra of the ALP + PPi + $MnFe_2O_4$ + TMB system with various activities of ALP (PPi: 5 mM; TMB: 0.25 mM; $MnFe_2O_4$: 25 μg mL^{-1}). **b** Depicts the linear relationship between the absorbance at 652 nm and the ALP activity. **c** Compares the UV–Vis responses of the developed assay toward different biological species (1—50 U L^{-1} ALP, 2—10 mM KCl, 3—10 mM Na_3PO_4, 4—1 mM cysteine, 5—1 mM glycine, 6—1 mM alanine, 7—1 mM glutathione, 8—5 mM bovine serum albumin, 9—5 mM glucose, 10—0.1 mM dopamine, 11—0.1 mM cholesterol, 12—50 U L^{-1} GOx, 13—10 U L^{-1} UOx, 14—10 U L^{-1} ChOx)

Table 1 Results of our assay for ALP determination in human serum samples

Sample	Measured by our assay ($n=3$, U L^{-1})	Clinical data (U L^{-1})	Relative error (%)
1#	53.4 ± 3.9	56	−4.6
2#	78.9 ± 3.7	77	+2.5
3#	48.7 ± 2.2	46	+5.9
4#	52.2 ± 3.1	53	−1.5

be utilized for signal readout [48]; (2) different from a majority of previously reported colorimetric approaches that depend on the optical changes of elements themselves [25, 62, 63], our assay is on the basis of the PPi-mediated activity switching of an oxidase-like nanozyme to catalytically amplify the colorimetric signal, and thus excellent sensitivity and low LOD are obtained. These merits will endow it with great promise in practical applications.

In addition to high sensitivity, the developed assay is also specific for ALP determination. We assessed the possible effects of common substances co-existing in human blood on the selective detection of ALP. As demonstrated in Fig. 5c, only ALP provides a remarkable absorbance at 652 nm, while other species, including inorganic salts (KCl and Na_3PO_4), amino acids (cysteine, glycine, and alanine), polypeptides (GSH), proteins (bovine serum albumin), small biological molecules (glucose, dopamine, and cholesterol), and natural enzymes (GOx, UOx, and ChOx), cannot trigger the restoration of the nanozyme-catalyzed TMB color reaction inhibited by PPi. The result confirms that our assay has good selectivity for the sensing of ALP. The excellent selectivity should be attributed to not only the exclusive inhibition of the $MnFe_2O_4$-catalyzed TMB color reaction by PPi but also the specific hydrolysis of PPi by ALP.

To evaluate the potential of our assay in practical applications, it was utilized to monitor the ALP levels in clinical samples. Four human serum samples available from the Affiliated Hospital of Jiangsu University were tested by our assay and compared with the clinical data. Since the normal level of ALP in adult serum ranges from 46 to 190 U L^{-1}, our assay is sensitive enough to detect the ALP levels in these samples directly. The detailed processes for real sample measurements have been described in the experimental section. The detection results are listed in Table 1. These results are found to be in agreement with the clinical data, providing the relative errors ranging from −4.6% to +5.9%. This indicates that our colorimetric assay can be used for the reliable determination of ALP in clinical practice.

4 Conclusions

In summary, we have developed a facile but effective colorimetric assay based on the PPi-mediated oxidase-mimicking activity switching of nanoscale $MnFe_2O_4$ for the determination of ALP. Our assay can provide enough sensitivity and specificity to sense ALP, and excellent reliability and practicability have also been verified by using it to monitor the target in practical samples. Taken together, our ALP assay shows great potential as a convenient, low-cost, and efficient tool in clinical practice, and the proposed strategy can also inspire the development of new ALP-linked immunosorbent assays.

Acknowledgements This study was supported by the National Natural Science Foundation of China (21605061 and 31601549), the Natural Science Foundation of Jiangsu Province (BK20160489), the Open Fund from the Shanghai Key Laboratory of Functional Materials Chemistry (SKLFMC201601), and the Cultivation Project for Excellent Young Teachers in Jiangsu University.

References

1. Reichling JJ, Kaplan MM. Clinical use of serum enzymes in liver disease. Dig Dis Sci. 1988;33:1601.
2. Furman R, Nicholas JJ, Jivoff L. Elevation of the serum alkaline phosphatase coincident with ectopic-bone formation in paraplegic patients. J Bone Jt Surg. 1970;52:1131.
3. Lorente JA, Valenzuela H, Morote J, et al. Serum bone alkaline phosphatase levels enhance the clinical utility of prostate specific antigen in the staging of newly diagnosed prostate cancer patients. Eur J Nucl Med. 1999;26:625.
4. Park KS, Lee CY, Park HG. A sensitive dual colorimetric and fluorescence system for assaying the activity of alkaline phosphatase that relies on pyrophosphate inhibition of the peroxidase activity of copper ions. Analyst. 2014;139:4691.
5. Deng JJ, Yu P, Wang YX, et al. Real-time ratiometric fluorescent assay for alkaline phosphatase activity with stimulus responsive infinite coordination polymer nanoparticles. Anal Chem. 2015;87:3080.
6. Xiao T, Sun J, Zhao JH, et al. FRET effect between fluorescent polydopamine nanoparticles and MnO_2 nanosheets and its application for sensitive sensing of alkaline phosphatase. ACS Appl Mater Interfaces. 2018;10:6560.
7. Li JY, Si L, Bao JC, et al. Fluorescence regulation of poly(thymine)-templated copper nanoparticles via an enzyme-triggered reaction toward sensitive and selective detection of alkaline phosphatase. Anal Chem. 2017;89:3681.
8. Song HW, Wang HY, Li X, et al. Sensitive and selective colorimetric detection of alkaline phosphatase activity based on phosphate anion-quenched oxidase-mimicking activity of Ce(IV) ions. Anal Chim Acta. 2018;1044:154.
9. Shi DM, Sun Y, Lin L, et al. Naked-eye sensitive detection of alkaline phosphatase (ALP) and pyrophosphate (PPi) based on a horseradish peroxidase catalytic colorimetric system with Cu(II). Analyst. 2016;141:5549.
10. Hu Q, Zhou BJ, Li F, et al. Turn-on colorimetric platform for dual activity detection of acid and alkaline phosphatase in human whole blood. Chem Asian J. 2016;11:3040.

11. Hayat A, Bulbul G, Andreescu S. Probing phosphatase activity using redox active nanoparticles: a novel colorimetric approach for the detection of enzyme activity. Biosens Bioelectron. 2014;56:334.
12. Jin LY, Dong YM, Wu XM, et al. Versatile and amplified biosensing through enzymatic cascade reaction by coupling alkaline phosphatase in situ generation of photoresponsive nanozyme. Anal Chem. 2015;87:10429.
13. Li CM, Zhen SJ, Wang J, et al. A gold nanoparticles-based colorimetric assay for alkaline phosphatase detection with tunable dynamic range. Biosens Bioelectron. 2013;43:366.
14. Hu Q, Zhou BJ, Dang PY, et al. Facile colorimetric assay of alkaline phosphatase activity using Fe(II)-phenanthroline reporter. Anal Chim Acta. 2017;950:170.
15. Yang JJ, Zheng L, Wang Y, et al. Guanine-rich DNA-based peroxidase mimetics for colorimetric assays of alkaline phosphatase. Biosens Bioelectron. 2016;77:549.
16. Liu Q, Li HX, Jin R, et al. Ultrasensitive detection alkaline phosphatase activity using 3-aminophenylboronic acid functionalized gold nanoclusters. Sens Actuators B. 2019;281:175.
17. Shi Y, Yang M, Liu L, et al. GTP as a peroxidase-mimic to mediate enzymatic cascade reaction for alkaline phosphatase detection and alkaline phosphatase-linked immunoassay. Sens Actuators B. 2018;275:43.
18. Ma JL, Yin BC, Wu X, et al. Copper-mediated DNA-scaffolded silver nanocluster on–off switch for detection of pyrophosphate and alkaline phosphatase. Anal Chem. 2016;88:9219.
19. Chen CX, Yuan Q, Ni PJ, et al. Fluorescence assay for alkaline phosphatase based on ATP hydrolysis-triggered dissociation of cerium coordination polymer nanoparticles. Analyst. 2018;143:3821.
20. Jia L, Xu JP, Li D, et al. Fluorescence detection of alkaline phosphatase activity with β-cyclodextrin-modified quantum dots. Chem Commun. 2010;46:7166.
21. Jiang H, Wang XM. Alkaline phosphatase-responsive anodic electrochemiluminescence of CdSe nanoparticles. Anal Chem. 2012;84:6986.
22. Goggins S, Naz C, Marsh BJ, et al. Ratiometric electrochemical detection of alkaline phosphatase. Chem Commun. 2015;51:561.
23. Ruan CM, Wang W, Gu BH. Detection of alkaline phosphatase using surface-enhanced Raman spectroscopy. Anal Chem. 2006;78:3379.
24. Dong J, Li Y, Zhang MY, et al. Ultrasensitive surface-enhanced Raman scattering detection of alkaline phosphatase. Anal Methods. 2014;6:9168.
25. Hu Q, He MH, Mei YQ, et al. Sensitive and selective colorimetric assay of alkaline phosphatase activity with Cu(II)-phenanthroline complex. Talanta. 2017;163:146.
26. Bowers GN, McComb RB. A continuous spectrophotometric method for measuring the activity of serum alkaline phosphatase. Clin Chem. 1966;12:70.
27. Babson AL, Greeley SJ, Coleman CM, et al. Phenolphthalein monophosphate as a substrate for serum alkaline phosphatase. Clin Chem. 1966;12:482.
28. Gao LZ, Zhuang J, Nie L, et al. Intrinsic peroxidase-like activity of ferromagnetic nanoparticles. Nat Nanotech. 2007;2:577.
29. Gao LZ, Yan XY. Nanozymes: an emerging field bridging nanotechnology and biology. Sci China Life Sci. 2016;59:400.
30. Wei H, Wang EK. Nanomaterials with enzyme-like characteristics (nanozymes): next-generation artificial enzymes. Chem Soc Rev. 2013;42:46060.
31. Wang XY, Guo WJ, Hu YH, et al. Nanozymes: next wave of artificial enzymes. Berlin: Springer; 2016.
32. Lin YH, Ren JS, Qu XG. Catalytically active nanomaterials: a promising candidate for artificial enzymes. Acc Chem Res. 2014;47:1097.
33. Wang XY, Hu YH, Wei H. Nanozymes in bionanotechnology: from sensing to therapeutics and beyond. Inorg Chem Front. 2016;3:41.
34. Wu JJX, Wang XY, Wang Q, et al. Nanomaterials with enzyme-like characteristics (nanozymes): next-generation artificial enzymes (II). Chem Soc Rev. 2019;48:1004.
35. Liu BW, Han X, Liu JW. Iron oxide nanozyme catalyzed synthesis of fluorescent polydopamine for light-up Zn^{2+} detection. Nanoscale. 2016;8:13620.
36. Xu XC, Zou XB, Wu SW, et al. In situ formation of fluorescent polydopamine catalyzed by peroxidase-mimicking FeCo-LDH for pyrophosphate ion and pyrophosphatase activity detection. Anal Chim Acta. 2019;1053:89.
37. Cao FF, Zhang Y, Sun YH, et al. Ultrasmall nanozymes isolated within porous carbonaceous frameworks for synergistic cancer therapy: enhanced oxidative damage and reduced energy supply. Chem Mater. 2018;30:7831.
38. Fan KL, Xi JQ, Fan L, et al. In vivo guiding nitrogen-doped carbon nanozyme for tumor catalytic therapy. Nat Commun. 2018;9:1440.
39. Huang YY, Liu Z, Liu CQ, et al. Self-assembly of multinanozymes to mimic an intracellular antioxidant defense system. Angew Chem Int Ed. 2016;128:6758.
40. Wang QQ, Wei H, Zhang ZQ, et al. Nanozyme: an emerging alternative to natural enzyme for biosensing and immunoassay. Trends Anal Chem. 2018;105:218.
41. Zhao J, Dong WF, Zhang XD, et al. FeNPs@Co_3O_4 hollow nanocages hybrids as effective peroxidase mimics for glucose biosensing. Sens Actuators B. 2018;263:575.
42. Niu XH, He YF, Pan JM, et al. Uncapped nanobranch-based CuS clews used as an efficient peroxidase mimic enable the visual detection of hydrogen peroxide and glucose with fast response. Anal Chim Acta. 2016;947:42.
43. Liu BW, Huang ZC, Liu JW. Boosting the oxidase mimicking activity of nanoceria by fluoride capping: rivaling protein enzymes and ultrasensitive F^- detection. Nanoscale. 2016;8:13562.
44. He YF, Niu XH, Shi LB, et al. Photometric determination of free cholesterol via cholesterol oxidase and carbon nanotube supported Prussian blue as a peroxidase mimic. Microchim Acta. 2017;184:2181.
45. He YF, Li X, Xu XC, et al. A cobalt-based polyoxometalate nanozyme with high peroxidase-mimicking activity at neutral pH for one-pot colorimetric analysis of glucose. J Mater Chem B. 2018;6:5750.
46. Hu YH, Cheng HJ, Zhao XZ, et al. Surface-enhanced Raman scattering active gold nanoparticles with enzyme-mimicking activities for measuring glucose and lactate in living tissues. ACS Nano. 2017;11:5558.
47. Niu XH, He YF, Zhang WC, et al. Elimination of background color interference by immobilizing Prussian blue on carbon cloth: a monolithic peroxidase mimic for on-demand photometric sensing. Sens Actuators B. 2018;256:151.
48. Zhang WC, Niu XH, Li X, et al. A smartphone-integrated ready-to-use paper-based sensor with mesoporous carbon-dispersed Pd nanoparticles as a highly active peroxidase mimic for H_2O_2 detection. Sens Actuators B. 2018;265:412.
49. He YF, Qi F, Niu XH, et al. Uricase-free on-demand colorimetric biosensing of uric acid enabled by integrated CoP nanosheet arrays as a monolithic peroxidase mimic. Anal Chim Acta. 2018;1021:113.
50. Liu SG, Han L, Li N, et al. A fluorescence and colorimetric dual-mode assay of alkaline phosphatase activity via destroying oxidase-like CoOOH nanoflakes. J Mater Chem B. 2018;6:2843.
51. Wang CH, Gao J, Cao YL, et al. Colorimetric logic gate for alkaline phosphatase based on copper(II)-based metal-organic

frameworks with peroxidase-like activity. Anal Chim Acta. 2018;1004:74.
52. Huang QW, He C, Zhang JL, et al. Unlocking the hidden talent of DNA: unexpected catalytic activity for colorimetric assay of alkaline phosphatase. Anal. Chim. Acta. 2019;1055:98.
53. Zhu X, Zhao HL, Niu XH, et al. A comparative study of carbon nanotube supported MFe2O4 spinels (M = Fe Co, Mn) for amperometric determination of H2O2 at neutral pH values. Microchim Acta. 2016;183:2431.
54. Vernekar AA, Das T, Ghosh S, et al. A remarkably efficient $MnFe_2O_4$-based oxidase nanozyme. Chem Asian J. 2016;11:72.
55. Liu J, Meng LJ, Fei ZF, et al. MnO_2 nanosheets as an artificial enzyme to mimic oxidase for rapid and sensitive detection of glutathione. Biosens Bioelectron. 2017;90:69.
56. Yan X, Song Y, Wu XL, et al. (2017) Oxidase-mimicking activity of ultrathin MnO_2 nanosheets in colorimetric assay of acetylcholinesterase activity. Nanoscale. 2017;9:2317.
57. Cheng HJ, Lin SC, Mahammad F, et al. Rationally modulate the oxidase-like activity of nanoceria for self-regulated bioassays. ACS Sens. 2016;1:1336.
58. Jiang B, Duan DM, Gao LZ, et al. Standardized assays for determining the catalytic activity and kinetics of peroxidase-like nanozymes. Nat Protoc. 2018;13:1506.
59. Xiang MH, Liu JW, Li N, et al. A fluorescent graphitic carbon nitride nanosheet biosensor for highly sensitive, label-free detection of alkaline phosphatase. Nanoscale. 2016;8:4727.
60. Chen CX, Lu LX, Zheng Y, et al. A new colorimetric protocol for selective detection of phosphate based on the inhibition of peroxidase-like activity of magnetite nanoparticles. Anal Methods. 2015;7:161–7.
61. Xue Q, Cao XY, Zhang CL, et al. Polydopamine nanodots are viable probes for fluorometric determination of the activity of alkaline phosphatase via the in situ regulation of a redox reaction triggered by the enzyme. Microchim Acta. 2018;185:231.
62. Gao ZQ, Deng KC, Wang XD, et al. High-resolution colorimetric assay for rapid visual readout of phosphatase activity based on gold/silver core/shell nanorod. ACS Appl Mater Interfaces. 2014;6:18243.
63. Yu L, Shi ZZ, Fang C, et al. Disposable lateral flow-through strip for smartphone-camera to quantitatively detect alkaline phosphatase activity in milk. Biosens Bioelectron. 2015;69:307.